Micro-Doppler Removal in Radar Imaging Analysis

Ljubiša Stanković[1], *Fellow, IEEE*, Thayananthan Thayaparan[2], *Senior Member, IEEE*, Miloš Daković[1], *Member, IEEE*, Vesna Popović-Bugarin[1], *Member, IEEE*

***Abstract*—The micro-Doppler effect is caused by fast moving reflectors. This effect may significantly decrease the readability of the ISAR/SAR images. An L-statistics based method for micro-Doppler effects removal is proposed in this paper. The L-statistics approach is performed on the spectrogram, while the rigid body signal synthesis is done in the complex time-frequency domain. The proposed method is very simple to use and produces better results than the other time-frequency based approaches. In addition to being capable of separating the rigid body and the micro-Doppler parts, this approach is robust to the noise influence. It may also separate close rigid body points, which are not separated in the original radar image. In the numerical implementation of this approach for the radar imaging, the computational efficiency is further improved by using two thresholds. The first threshold determines whether there is a target signal in a range cell, while the second threshold determines whether there are micro-Doppler effects in this range cell. These thresholds could significantly decrease the computation time in real-time applications. Theory is illustrated by examples.**

***Index Terms*—Radar imaging, ISAR/SAR, micro-Doppler, L-statistics, time-frequency analysis, short-time Fourier transform.**

I. Introduction

The micro-Doppler (m-D) effect appears in the inverse synthetic aperture radar (ISAR) imaging when a target has one or more fast moving parts [1]-[7]. Similar effect appears in the synthetic aperture radar (SAR) imaging, as well, [8]. This effect may decrease the readability of radar images. The frequency content of the m-D signal changes over time in a wide range. Therefore, the m-D may cover the rigid body and make it difficult to detect. On the other hand, the m-D effect, at the same time, carries useful information about the features of moving parts (type, velocity, size, etc.) [9]. It is easier to estimate these features if the m-D effect is separated from the rigid body part of the radar image. Thus, the extraction of m-D effects from the radar images has attracted significant research attention. High-resolution linear and quadratic time-frequency (TF) analysis techniques have been used for extracting the m-D features. In [8], TF signatures of oscillating corner reflector are obtained by using an adaptive optimal kernel in distributions from the Cohen's class. The wavelet analysis of helicopter and human data, along with the TF representation based imaging system, is used in [10], [11]. A method for separating the m-D effect from the radar image, based on the chirplet transform, has been proposed in [12]. Both, wavelet-based and chirplet-based procedures are used in [13] to extract the m-D parameters, such as the rotating frequency of an antenna in the SAR data. However, the effectiveness of the chirplet-based methods is dependent on the selection of the number of chirplets used in decomposition. Its calculation burden is also high, since the chirplet dictionary could be extremely large. Recently, two additional techniques for the target's rigid body separation from the m-D parts have been proposed in [14]. The first technique is based on the order statistics of the spectrogram samples. The second one is based on the inverse Radon transform processing of the obtained radar signals. An efficient TF based approach, in conjunction with the Viterbi algorithm, is proposed in [15] for the extraction of the m-D features.

In this paper, we use the L-statistics based approach for the rigid body separation. In order to remove the m-D effect, we perform the TF analysis within the coherent integration time (CIT). In our previous approach [14], we used order statistics and several TF representations with various windows. The obtained TF representations were then used to make decision whether a component belongs to the rigid body or to the fast moving target point. Here, we use only one window function in the analysis. Order statistics is performed based on the spectrogram, while the rigid body signal synthesis is done in the complex TF domain. This approach is very simple to use and produces better results than the other approaches. It is also robust to the noise influence, since it uses the L-statistics, being known as a robust signal processing tool [16]. The L-statistics application to the complex STFT leads to a form of super-resolution representation, as well. It can separate very close rigid body components, even when that is not possible by using the standard Fourier transform (FT) over the entire CIT. The proposed method can be easily adapted for efficient compensation of a residual, uncompensated, rigid body acceleration in the presence of the m-D effects.

In order to improve the calculation efficiency, we have proposed a procedure to establish whether there is any target return in a considered range bin. Moreover, by bearing in mind that in the ISAR/SAR analysis only some range bins may contain the m-D effect, while most of the range bins are m-D free, in this paper we have defined a criterion for detecting ranges which contain the m-D effects. The m-D removal procedure could be performed only for these

[1] University of Montenegro, Electrical Engineering Department, 81000 Podgorica, Montenegro, E-mail: {ljubisa,milos,pvesna}@ac.me.

[2] Radar Applications and Space Technologies, Defence R&D Canada – Ottawa, Ottawa, Ontario, Canada, E-mail: Thayananthan.Thayaparan@drdc-rddc.gc.ca.

particular range bins.

The paper is organized in five Sections. In Section II, the radar signal model is presented, including the model of rigid body points and fast moving reflectors. The drawbacks of the FT, in the case of fast moving reflector imaging, are analyzed, as well. The rigid body separation, based on the L-statistics, is proposed in Section III. It is presented in a form of an algorithm. The robustness to noise and high resolution property of the proposed procedure are discussed here. Simulation and experimental results are given in Section IV.

II. Radar Signal Model

Consider a continuous wave (CW) radar that transmits a signal in the form of a coherent series of M chirps [17]. The received signal, reflected from a target, is delayed with respect to the transmitted signal for $t_d = 2d(t)/c$, where $d(t)$ is the target distance from the radar and c is the speed of light. This signal is demodulated to baseband, with possible distance compensation and other preprocessing operations (such as pulse compression). In order to analyze the influence of cross-range non-stationarities in the radar imaging, we will consider only the Doppler part in the received signal of a point target, in the continuous dwell time, as it is usually done in the radar literature [17],

$$s(t) = \sigma e^{j2d(t)\omega_0/c}, \tag{1}$$

where σ is the reflection coefficient of the target, while ω_0 is the radar operating frequency. The repetition time of a single chirp will be denoted by T_r, while the number of samples within each chirp is N. The CIT is $T_c = MT_r$. The received signal, for a system of point scatterers, can be modeled as a sum of individual point scatterer responses, [17].

A. ISAR Setup

In the ISAR case, the aim is to obtain a high-resolution image of a target based on the change in viewing angle of the target with respect to the fixed radar. The common ISAR imaging models assume that all point scatterers share the same angular motion, Fig.1(a). Then, the Doppler part of the received signal, within the m-th radar sweep, corresponding to the K rigid body points, can be written as, [12], [17]:

$$s(t) = \sum_{i=1}^{K} \sigma_{Bi} e^{j2[R_B(t) + x_{Bi}\cos(\theta_B(t)) + y_{Bi}\sin(\theta_B(t))]\omega_0/c}, \tag{2}$$

where the target's translation and angular motion are denoted by $R(t)$ and $\theta(t)$. For each point we have used an approximation $d_i(t) = \sqrt{(R(t)+x_i)^2 + y_i^2} \cong R(t) + x_i$ to obtain $d_{Bi}(t) \cong R_B(t) + x_{Bi}\cos(\theta_B(t)) + y_{Bi}\sin(\theta_B(t))$. Index $_B$ is added to denote the rigid body parameters. The initial locations of points, in the coordinate system whose origin is in the center of the target rotation, are (x_{Bi}, y_{Bi}), Fig.1(a).

For the rigid body points $|\theta_B(t)| \ll 1$ holds, during the CIT, following in $\cos\theta_B(t) \approx 1$ and $\sin\theta_B(t) \approx \theta_B(t) = \omega_B t$, where ω_B is the effective body rotation rate, after the motion compensation. Motion compensation techniques [12], [18] are employed to remove the influence of the translation motion, thus we can also neglect the remaining factor $R_B(t) + x_{Bi}$.

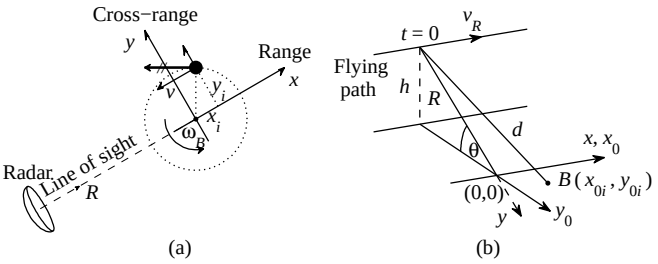

Fig. 1. (a) Geometry of the ISAR system. (b) Geometry of the SAR system

The previous approximations cannot be applied for fast rotating (moving) points, since their angular position $\theta_R(t)$ can significantly change during the CIT. Index $_R$ will be used for fast moving points. Assume that there are P fast rotating points, which rotate around their central points (x_{R0i}, y_{R0i}) with radii A_{Ri}. Coordinates of these points are described by $x_p = x_{R0i} + A_{Ri}\sin(\theta_R(t))$ and $y_p = y_{R0i} + A_{Ri}\cos(\theta_R(t))$. Thus, the resulting coordinate changes of these scatterers are:

$$\begin{bmatrix} x_p' \\ y_p' \end{bmatrix} = \begin{bmatrix} \cos\theta_B(t) & \sin\theta_B(t) \\ -\sin\theta_B(t) & \cos\theta_B(t) \end{bmatrix} \begin{bmatrix} x_p \\ y_p \end{bmatrix}. \tag{3}$$

Assume now that the rotation speed of the i-th fast rotating point is ω_{Ri}, with $\theta_{Ri}(t) = \omega_{Ri} t$. With the previous approximations for the rigid body values, after compensation for $R(t)$ and x_{R0i}, we have:

$$d_i(t) \cong y_{R0i}\omega_B t + A_{Ri}\sin(\omega_{Ri} t). \tag{4}$$

The received signal, including both the rigid body points and the fast rotating m-D points, can be written as:

$$s(t) = \sum_{i=1}^{K} \sigma_{Bi} e^{j2y_{Bi}\omega_B t\omega_0/c} + \sum_{i=1}^{P} \sigma_{Ri} e^{j2[y_{R0i}\omega_B t + A_{Ri}\sin(\omega_{Ri} t)]\omega_0/c}. \tag{5}$$

A similar form of the received signal is obtained in the case of vibrating points. If a reflecting point vibrates, around a central point (x_{R0i}, y_{R0i}), along a line parallel to the line-of-sight, with frequency ω_{Vi}, reaching the maximum amplitude A_{R_i} from the central point, then we get the form as (5), with the last phase term $A_{Ri}\sin(\omega_{Ri} t)$ being replaced by $A_{Ri}\sin(\omega_{Vi} t)$. Thus, the vibrations can be analyzed in the same way as the rotations. The m-D points may not make a whole period within the CIT, or may be aperiodic in nature. Any other arbitrary motion can easily be described within the previous framework, by using $x_p = x_{R0i} + x_{arb}(t)$ and $y_p = y_{R0i} + y_{arb}(t)$ in (3). The theory presented next, can be used in these cases, as well.

Since we will consider only the Doppler component part in the received signal, the analysis of the radar signal

reduces to one-dimensional signal (5) and its FT, $S(\Omega) = FT\{s(t)\}$, analysis. In the discrete form, the FT reads:

$$S(k) = \sum_{i=0}^{M-1} s(i) e^{-j2\pi ik/M}. \quad (6)$$

Its squared absolute value $|S(k)|^2$ is called the periodogram. If we calculate the FT of the signal corresponding to one point of the rigid body in (5), we get

$$S_{Bi}(\Omega) = FT\left\{\sigma_{Bi} e^{j2y_{Bi}\omega_B t\omega_0/c}\right\} = 2\pi\sigma_{Bi}\delta(\Omega - \frac{2\omega_0}{c}\omega_B y_{Bi}).$$

It is a delta pulse at the position proportional to the cross-range coordinate y_{Bi}. The delta pulse position depends not only on the radar parameters, that are constant, but also on the rotation speed ω_B.

The Doppler part of the radar signal that corresponds to an arbitrary moving point is a frequency modulated signal with the instantaneous frequency

$$\Omega_{Ri}(t) = \frac{2\omega_0}{c}[y_{R0i}\omega_B + d(x_{arb}(t))/dt], \quad (7)$$

with approximations as in the derivation of (4) and (5). Note that relations (2) and (3), without any approximation, can be used in simulations, instead of the presented compact form (5) that is appropriate for the qualitative analysis. For pure rotation, we have $d(x_{arb}(t))/dt = A_{Ri}\omega_{Ri}\cos(\omega_{Ri}t)$.

The constant part in (7) corresponds to the center of the fast moving point. It is proportional to the rigid body rotation speed, $y_{R0i}\omega_B$. However, for the rotation the resulting rate $\omega_{Ri} = \theta'_{Ri}(t)$ of this point is significantly higher than the rotating rate of the rigid body ω_B. Corresponding instantaneous frequency is $\Omega_{Ri}(t) = \frac{2\omega_0}{c}[y_{R0i}\omega_B + A_{Ri}\omega_{Ri}\cos(\omega_{Ri}t)]$. The radar image of the fast rotating reflectors spreads over a frequency interval, defined by the instantaneous frequency changes $2\omega_0 A_{Ri}\omega_{Ri}\cos(\omega_{Ri}t)/c$. The frequency interval width is proportional to the rotating speed and the target geometry. The scale factor for the radar image of the rotating reflector is ω_{Ri}. It is different from the scale factor of the radar image of the rigid body ω_B. Thus, the relative locations of the fast rotating parts are in a different scale with respect to the rigid body points. The ratio of the scales is $F \simeq \omega_{Ri}/\omega_B$. In order to obtain the radar image, with the rigid body and rotating reflectors, depicted as if they do not perform rotation, we should separate them, reconstruct the FT of rotating reflectors, re-scale it so that it is with the same scale as the FT of the rigid body, and put it back in the FT of the rigid body.

The presented analysis could be generalized on any fast movement within the CIT, including cases when the m-D part assumes the form of linear frequency modulated chirps. As long as the instantaneous frequency changes of the m-D points are faster than those of rigid body points (in an ideal case the last one should not change), the theory that we will present next, could be applied.

B. SAR Setup

Consider a SAR setup, as in Fig.1(b). First assume that the radar movement is parallel to the imaged terrain. This position of the radar will be described by the elevation angle $\theta = 0$. Denote the radar speed as $\vec{v}_R$ and assume that it moves in a direction of the x_0 axis of the coordinate system, $\vec{v}_R = v_R\vec{i}_{x_0}$. Assume that the line-of-sight is in the direction of y_0 axis, with unity vector $\vec{i}_{y_0}$. The distance of the radar to the center of the imaged terrain is denoted by $\vec{R}_0 = R_0\vec{i}_{y_0}$. At one instant, the radar movement corresponds to the rotation of the terrain, with respect to the radar, with $\vec{\omega}_B = \vec{R}_0 \times \vec{v}_R = R_0 v_R \vec{i}_{z_0}$.

Now assume that there is only one stationary reflecting point, located at (x_{0i}, y_{0i}, z_{0i}). Taking into account that the image plane with the reflecting point rotates with $\vec{\omega}_B$ around the central point, point movement (trajectory) can be described by a simple rotation matrix. Consequently, the signal $s_i(t)$ reflected from this point, bearing in mind that the distance R_0 is much greater than any reflecting point coordinate, can be written as:

$$s_i(t) \cong \sigma_i e^{j(-x_{0i}\sin(\omega_B t) + y_{0i}\cos(\omega_B t))\omega_0/c}, \quad (8)$$

where the constant phase terms $\exp(j2\omega_0 R_0/c)$ is omitted. In the sequel, we will use equality sign in (8) for simplicity of notation.

In general, if the radar is at $\theta \neq 0$, we have a new coordinate system, related to the radar, in which the initial positions of the reflecting points are rotated for θ angle around the x_0 axis, Fig.1(b), as $x_{0i}(\theta) = x_{0i}$, $y_{0i}(\theta) = y_{0i}\cos(\theta) - z_{0i}\sin(\theta)$ and $z_{0i}(\theta) = y_{0i}\sin(\theta) + z_{0i}\cos(\theta)$. The rotation in this coordinate system, then remains the same as for $\theta = 0$, with rotation vector $\vec{\omega}_B = R\vec{i}_y \times v_R\vec{i}_x = R_0 v_R\vec{i}_z = \omega_{B\theta}\vec{i}_z$. The resulting rotation is: $x_i(t) = x_{0i}\cos(\omega_{B\theta}t) + y_{0i}(\theta)\sin(\omega_{B\theta}t)$, $y_i(t) = -x_{0i}\sin(\omega_{B\theta}t) + y_{0i}(\theta)\cos(\omega_{B\theta}t)$ and $z_i(t) = y_{0i}\sin(\theta) + z_{0i}\cos(\theta)$. The signal $s_i(t)$ is of the form

$$s_i(t) = \sigma_i e^{j2(-x_{0i}\sin(\omega_{B\theta}t) + [y_{0i}\cos(\theta) - z_{0i}\sin(\theta)]\cos(\omega_{B\theta}t))\omega_0/c}. \quad (9)$$

Assume now that in addition to the pure rotation, caused by radar movement, the point has a fast arbitrary movement around (x_{0i}, y_{0i}, z_{0i}), described by $x_i(t) = x_{0i} + x_{arb}(t)$, $y_i(t) = y_{0i} + y_{arb}(t)$ and $z_i(t) = z_{0i} + z_{arb}(t)$, where index $_{arb}$ is used to denote such a movement. With approximation $\omega_{B\theta}t \ll 1$, appropriate distance compensation and by neglecting constant phase terms, we get

$$s_i(t) \cong \sigma_i e^{j2[-x_{0i}\omega_{B\theta}t + [y_{arb}(t)\cos(\theta) - z_{arb}(t)\sin(\theta)]]\omega_0/c}.$$

For a special case of rotation in the x_0Oy_0 plane, with $x_i(t) = x_{0i} + A_i\sin(\omega_{R_i}t)$, $y_i(t) = y_{0i} + A_i\cos(\omega_{R_i}t)$ and $z_i(t) = 0$, the corresponding instantaneous frequency is

$$\Omega_i(t) = \frac{2\omega_0\omega_{B\theta}}{c}[-x_{0i} - A_i\frac{\omega_{R_i}}{\omega_{B\theta}}\sin(\omega_{R_i}t)\cos(\theta)]. \quad (10)$$

In this way, we have modeled an experiment with a pendulum caused m-D in the SAR, when $\theta_p(t) = \theta_{p0}\cos(\sqrt{g/l}\,t)$, with θ_{p0} being the pendulum maximal angle and g is the gravity acceleration. For a pendulum with the center located at $(0,0,l)$ oscillating in xOy plane

we can derive $y_{arb}(t) = l\sin\theta_p(t)$, $z_{arb}(t) = l - l\cos\theta_p(t)$ and $x_{arb}(t) = 0$.

In simulations, the original form (9), without approximations, may produce more accurate results.

We can conclude that, in the following analysis, the ISAR and the SAR setup can be considered in a unified way.

III. Time-frequency Analysis and L-statistics

A simpler way to localize the signal behavior in shorter intervals, within the CIT, is in applying a window function to the standard FT. The resulting short-time Fourier transform (STFT) is defined as

$$STFT(t,\Omega) = \int_{-\infty}^{\infty} s(\tau)\, w(\tau - t) e^{-j\Omega\tau} d\tau, \tag{11}$$

or in a discrete form

$$STFT(m,k) = \sum_{i=0}^{M-1} s(i)\, w(i-m) e^{-j2\pi ik/M}, \tag{12}$$

where $w(i)$ is a window function used to truncate the considered signal. The squared absolute value of the STFT is called the spectrogram. In most of the provided examples, we will use a Hann(ing) window. The window width is M_w, $w(i) \neq 0$ for $-M_w/2 \leq i \leq M_w/2 - 1$. In our applications, the window is zero padded up to M, the same number of samples as in (6), so that we have the same frequency grid in the STFT as in the FT. Then, we can later easily reconstruct the FT, without interpolation, with the concentration close or equal to the concentration of the original FT. We know that, by using a lag window $w(i)$ in the STFT, the concentration in frequency is reduced, as compared to the original FT (6). For example, if the lag window width is M_w, then the concentration of a sinusoidal signal is reduced M/M_w times, i.e., the STFT-based ISAR/SAR image of a rigid body point (the main lobe of the FT of a sinusoid) would be approximately M/M_w times wider than the original FT based image of the same reflecting point. We will also refer to this effect as: the concentration being M/M_w times lower in the STFT than in the original FT.

A. Restoring the High FT Concentration from the STFT

The concentration could be restored to the original one by summing all the low concentrated STFT (complex) values over m. Since we calculated $STFT(m,k)$ with the window of the width M_w, there are two possibilities for its summation: (a) For all time instants $0 \leq m \leq M-1$, when the signal $s(i)$ has to be zero-padded for $-M_w/2 \leq i < 0$ and $M \leq i < M + M_w/2 - 1$; (b) For instants $M_w/2 \leq m \leq M - M_w/2$, when zero-padding of $s(i)$ is not used. Reconstruction formula, for the case when the signal is not zero-padded, is

$$\sum_{m=M_w/2}^{M-M_w/2} STFT(m,k) = \tag{13}$$
$$\sum_{i=0}^{M-1} s(i) \left[\sum_{m=M_w/2}^{M-M_w/2} w(i-m) \right] e^{-j2\pi ik/M}$$
$$= \sum_{i=0}^{M-1} s(i)\, w_1(i) e^{-j2\pi ik/M} = S_{w_1}(k).$$

In the case when the STFT is calculated for each time instant (time step one in the STFT calculation), the resulting window $w_1(i)$ is constant, $w_1(i) = const$, for $M_w - 1 \leq i \leq M - M_w$, for any window. It means that during the most of the CIT interval we have the normalized resulting window $w_1(i)$ being close to the rectangular one, with a small transition at the ending M_w points. The FT of the window obtained during the process of reconstruction produces a concentration very close to the full range rectangular window case (i.e., no window). It means that we will be able to reconstruct the FT with a concentration close to the one in the original FT (6), by using low concentrated STFTs, calculated with narrow windows. In this way, we will restore the high concentrated radar image, although we used low concentrated STFT in the analysis. The transition at the ending points of $w_1(i)$ can be easily overcome by zero padding the analyzed signal $s(i)$ with $M_w/2$ samples on both sides, (as explained before). Then, the pure rectangular window $w_1(i)$ would be obtained, for any window $w(i)$. The analysis is not restricted to the step one in the STFT calculation. The same resulting window would be obtained for a step equal to a half of the window width ($M_w/2$) and a Hann(ing), Hamming, triangular or rectangular window. The same is valid for steps equal to $M_w/4$, $M_w/8$, etc.

In order to explain how this mechanism of restoring the original concentration, by summing low-concentrated images, works, consider $s(t) = \exp(j\omega_0 t)$. Its FT is a delta pulse $S(\Omega) = 2\pi\delta(\Omega - \omega_0)$. The STFT of this signal produces

$$STFT(t,\Omega) = W(\Omega - \omega_0)\exp(j(\Omega - \omega_0)t). \tag{14}$$

Let us now analyze the result of summing the STFT values over t:

For $\Omega = \omega_0$, constant values of $W(0)$ will be integrated over an infinite time interval, with the phase $\exp(j(\Omega - \omega_0)t) = \exp(j0)$, producing $\int_{-\infty}^{\infty} STFT(t,\Omega)dt \to \infty$ for $\Omega = \omega_0$.

For any other Ω not equal to ω_0, i.e., when $\Omega = \omega_0 + \theta$, $\theta \neq 0$, we will have the integration $\int_{-\infty}^{\infty} W(\theta)\exp(j\theta t)dt = W(\theta)\int_{-\infty}^{\infty}\exp(j\theta t)dt = 0$. Therefore, all values for $\Omega \neq \omega_0$ are averaged out to zero by summation of the low concentrated STFTs over time.

The discrete form of (14), is

$$S(k) = \sum_{m=0}^{M-1} W(k - k_0) e^{j2\pi m(k-k_0)/M} \tag{15}$$

with the same conclusions as in the continuous case. Values of $S(k)$, when the signal is not zero-padded, are close to (15).

B. Basic Idea for the Separation of a Rigid Body and Fast Rotating Part

The presented mechanism of restoring the original concentration of the FT, in conjunction with the knowledge of the TF behavior patterns of fast moving and rigid scattering points, lead us to an algorithm for the m-D free, highly concentrated, radar image. The rigid body and the fast moving points behave differently in the TF representation

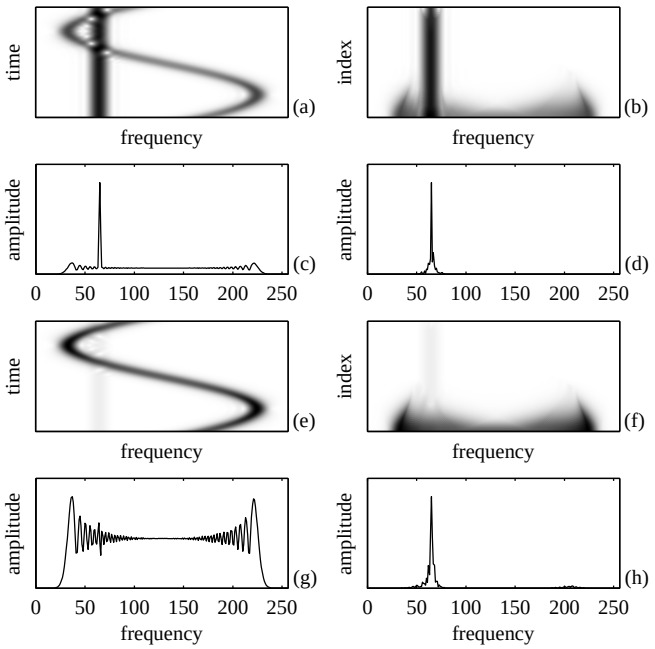

Fig. 2. Simulated radar signals which correspond to a rigid body reflector with $\sigma_B = 1$ and a rotating reflector with reflection coefficient $\sigma_R = 0.8$: a) Absolute value of the STFT, b) Sorted STFT values, c) The original FT, and d) The reconstructed FT. Simulated radar signals which correspond to a rigid body reflector with $\sigma_B = 1$ and a rotating reflector with reflection coefficient $\sigma_R = 15$: e) Absolute value of the STFT, f) Sorted STFT values, g) The original FT, and g) The reconstructed FT.

of the returned radar signal, within the CIT. The rigid body signal is almost constant in time (stationary), while the fast-varying m-D part of the signal is highly non-stationary. This part of signal keeps changing its position in the frequency direction.

For the illustration, let us assume that the signal is returned from one point of a rigid body scatterer and one point of a fast rotating (m-D) scatterer. We analyze two cases with different strengths of the m-D reflection. In the first case, the reflection coefficient of the rigid body is $\sigma_B = 1$, while the reflection coefficient of the fast moving scatterer is $\sigma_R = 0.8$. The STFT representation of the resulting signal is shown in Fig.2(a). The second case is with a strong m-D, $\sigma_R = 15$ and the same σ_B as in the previous case. The STFT representation of this signal is shown in Fig.2(e). In both cases, the rigid body part is at a constant frequency for all t within the CIT, while the fast rotating part changes frequency. If we perform sorting over the time axis, as in Figs2(b,f), we will not change the result of the summation in (13) since it is a commutative operation. By summing the STFT values over time, from either of these two plots, presented in Fig.2(a,b) or Fig.2(e,f), we will get the original FT of the corresponding signal Fig.2(c,g). Note that any value of σ_R from (and including the case without m-D) $\sigma_R = 0$ up to $\sigma_R \gg \sigma_B$ will not significantly change the pattern.

The basic idea for separating the rigid body and the fast rotating part is in the sorting of STFT values of the returned radar signal along the time axis, within the CIT. Since the rigid body return is stationary, the sorting procedure will not significantly change the distribution of its values. However, the fast-varying m-D part of the signal is highly non-stationary, occupying different frequency bins for different time instants (in the case of flashes it exists for some time-instants only). Its existence is short in time, for each frequency, over a wide range of frequencies. Thus, after sorting the STFT along the time axis, the m-D part of the signal has strong values over a wide frequency range, but for a few samples only. By removing several large amplitude values of the sorted STFT, for each frequency, we eliminate most or all of the m-D part of the signal. Summing the rest of the STFT values over time we will get the rigid body radar image. The sinusoidal m-D pattern, presented in Fig.2, is just an example of such a signal. This idea can be applied on any non-stationary signal form. The m-D part of a signal is non-stationary by definition.

Let us consider a set of M (or $M-M_w$ if the signal is not zero-padded) elements of the STFT, for a given frequency k,

$$\mathbf{S}_k(m) = \{STFT(m,k), m = 0,1,...,M-1\}.$$

After sorting $S_k(m)$ along the time, for a given frequency k, we obtain a new ordered set of elements $\Psi_k(m) \in S_k(m)$ such that $|\Psi_k(0)| \le |\Psi_k(1)| \le .... \le |\Psi_k(M-1)|$. Of course, the addition is commutative operation, so if we use the whole set, we get

$$\sum_{m=0}^{M-1} STFT(m,k) = \sum_{m=0}^{M-1} \Psi_k(m) = S(k).$$

In the L-statistics form of this summation we will, for each k, omit $M-M_Q$ of the highest values of $\Psi_k(m)$ and produce the L-estimate of $S(k)$, denoted by $S_L(k)$, as

$$S_L(k) = \sum_{m=0}^{M_Q-1} \Psi_k(m) \tag{16}$$

where M_Q =int$[M(1-Q/100)]$ and Q is the percent of omitted values.

To illustrate this procedure, we eliminated 40% of the top amplitude values of the STFT from the previous example. In this way, we completely eliminated the m-D component from the TF representation. We are left with 60% of the low amplitude values of the STFT, that contain only the rigid body. The FT reconstruction is performed based on these values only. The reconstructed FTs for the cases of a weak and a strong m-D are shown in Fig.2(d,h), respectively. The FT of the rigid body is in both cases successfully reconstructed by summing 60% of the sorted STFT samples, remained after m-D separation. Note that the result is not significantly influenced by the value of σ_R, since the points corresponding to the m-D signature are removed, meaning that their values are almost not important.

In the data analysis, this approach, based on elimination of a part of data, before analyzing the rest of the data, is known as the L-statistics [16].

1) Analysis of the Missing Values: Since we have eliminated some of the TF representation (TFR) values, we will analyze the influence of incomplete sum in (13). This is the same theory like the L-statistics theory applied to the noisy or non-noisy data, [16].

Assume that only points in $m \in D_k$ are used in summation:

$$S_L(k) = \sum_{m \in D_k} STFT(m,k), \tag{17}$$

where, for each k, D_k is a subset of $\{0,1,2,...,M-1\}$ with M_Q elements**.**

Within the framework of the previous analysis, it means that there will be a highly concentrated component $S(k)$ surrounded by several low-concentrated values $\sum_{m \notin D_k} STFT(m,k)$. Note that the amplitude of $STFT(m,k)$ is M times lower than the amplitude $S(k)$, since $S(k)$ is obtained as a sum of M values of the STFT. In general, by removing let say $(M-M_Q)$ values in m, we will get one very highly concentrated pulse, as in $S(k)$, and $(M-M_Q)$ values of low-concentrated components of the type $STFT(m,k)$, being spread around the peak of $S(k)$ and summed up by different random phases. Only the peak value is summed in phase. Consider:

1. Case for $k = k_0$ corresponding to the position of the rigid body point: At this frequency, all terms in the sum (15) are the same and equal to $W(0)$. Thus, the value of $S_L(k)$ does not depend on the positions of the removed samples. Its value is $S_L(k_0) = M_Q W(0)$.

2. Case for $k = l + k_0$, where $l \neq 0$: Removed terms in (15) are of the form $\mathbf{x}_l(m) = W(l)e^{j2\pi ml/M}$. They assume values from the set $\Phi_l = \{W(l)e^{j2\pi ml/M},\ m = 0,1,2,...,M-1\}$, with equal probability, for a given l. The statistical mean of these values is $E\{\mathbf{x}_l(m)\} = 0$ for $l \neq 0$, resulting in $E\{S_L(l+k_0)\} = 0$.

The resulting statistical mean for any k is

$$E\{S_L(k)\} = M_Q W(0)\delta(k-k_0).$$

The higher order statistical analysis of this process could be performed in detail, but it is out of the scope of this paper. Here, the influence of the number of missing points to the concentration of the reconstructed FT will be illustrated by an example, Fig.3. Here we consider a constant frequency signal, without m-D. Its FT is calculated and presented in Fig.3(a). Then the FT is reconstructed based on 25%,50% and 75% of the low amplitude values of the STFT for each k. We can see that even by taking a small number of STFT points, we still keep a strong peak, since it is summed in phase, Fig.3(b),(c),(d).

2) Noise Influence: It is well known [16] that the L-statistics is a tool for robust time-frequency analysis. The robustness comes from the fact that the L-statistics based calculation avoids highest values, which are the most influenced by noise. Therefore, we may expect that by using the L-statistics we will not degrade the radar imaging performance in the case of noise. By using the L-statistics we will eliminate a part of the signal, that is summed in phase in the FT, but we will also eliminate the signal values that are mostly corrupted by noise. Thus, with the elimination of the m-D we will improve the overall performance in the noisy signal cases, as well. In the case of impulse noise, we may expect significant improvement, even in the case without m-D, with a pure rigid body. The effect of noise is statistically analyzed within the simulation study of this paper.

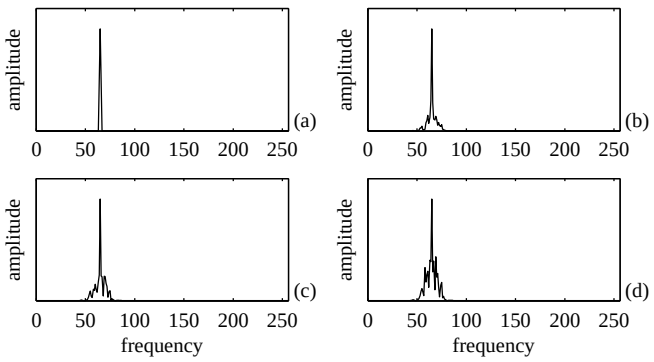

Fig. 3. The FT of a sinusoidal signal: (a) Original, (b) Reconstructed by summing 75% of the smallest STFT values, for each k, (c) Reconstructed by summing 50% of the smallest STFT values, (d) Reconstructed by summing 25% of the smallest STFT values.

3) High-Resolution Property: Consider the L-statistics application on two very close rigid body points:

$$s(t) = e^{-j2(y_{Bi}-\Delta y_{Bi})\omega_B t\omega_0/c} + e^{-j2(y_{Bi}+\Delta y_{Bi})\omega_B t\omega_0/c}$$

with a very small Δy_{Bi} so that in the FT of the signal $S(\Omega)$, calculated over the entire CIT, we can not distinguish these components. Since the resolution in the Doppler direction is $R_{Dopp} = 2\pi/T_c$ it means $2\Delta y_{Bi} \sim 2\pi/T_c$.

It is surprising, but if we use low concentrated STFT and the proposed L-statistics, we will be able to separate these components. The STFT of these components is

$$STFT(t,\Omega) = W(\Omega + (y_{Bi}-\Delta y_{Bi}))e^{-j\Omega t}e^{-j(y_{Bi}-\Delta y_{Bi})t} + W(\Omega + (y_{Bi}+\Delta y_{Bi}))e^{-j\Omega t}e^{-j(y_{Bi}+\Delta y_{Bi})t}$$

with normalized frequency Ω for $2\omega_0\omega_B/c = 1$.

Note that the STFTs of the components are phase shifted for $\Delta\varphi(t) = 2\Delta y_{Bi}t$. Even for small $2\Delta y_{Bi} \sim 2\pi/T_c$ the phase shift changes are of the order $\Delta\varphi(t) \sim 2\pi/T_c \times T_c$. It means that it could easily change, during the CIT, between 0 and π or even more. Then, there will be time instants in $|STFT(t,\Omega)|$ when the individual STFTs are summed in phase, i.e., when $|STFT(t,\Omega)| \cong \left|W(\Omega + (y_{Bi}-\Delta y_{Bi})) + W(\Omega + (y_{Bi}+\Delta y_{Bi}))\right|$. Then the signal components can not be separated. However, there will be also the instants in the STFT when the components are with opposite phase, $|STFT(t,\Omega)| \cong \left|W(\Omega + (y_{Bi}-\Delta y_{Bi})) - W(\Omega + (y_{Bi}+\Delta y_{Bi}))\right|$, so that the signal components are clearly separated. We can see that in the first case the values of $|STFT(t,\Omega)|$ will be higher than in the other case. By using the L-statistics approach the higher values will be eliminated, while the lower values, that are well separated, will remain. Thus, we may achieve high signal resolution by using the low concentrated STFT

and the L-statistics, even in the case when the separation is not possible in the original FT over the whole CIT.

C. Adaptive Percentage of Missing Values

There are two possible approaches to establish the threshold for the elimination of the m-D:

The first approach is to assume a fixed threshold for the entire ISAR/SAR image: for example, removing Q[%] highest values for each frequency, by knowing that this will not disturb significantly the obtained image.

A more sophisticated approach is to calculate the adaptive threshold for each range. The adaptive threshold can be obtained based on the L-statistics. To use the L-statistics approach, we will sort the STFT values for a given range and a given frequency. If there is a m-D, then, after sorting the STFT values, there is a region of an increase of the sorted STFT values, Fig.4 (upper part). Thus, if we sum the sorted STFT values over frequency, we will get a function:

$$A(m) = \sum_{k} |\Psi_k(m)|^2 . \tag{18}$$

Now, we can find the reference level R_L based on the mean of 10% of the low ampliude samples, i.e., based on $M/10$ values of the sorted $\Psi_k(m)$, $R_L = T_{hr} \sum_{m=0}^{M/10-1} 10A(m)/M$,with T_{hr} being a parameter, usually from $T_{hr} = 2$ to $T_{hr} = 10$. For example, $T_{hr} = 2$ means that we will use all the values in the sorted $\Psi_k(m)$ whose squared values are up to, for example, 2 times greater than mean of 10% lowest squared values. Then Q is found as the percent of $A(m)$ below R_L. In the case when there is no m-D it means that we will use all the values, since the stationary values are close to the mean of the lowest values for all time instants. If there is a m-D then the value outside of the stationary points will start to increase sharply and the summation will stop. The results are not too sensitive to these values, since $A(m)$ is a fast increasing function when the m-D starts to appear, Fig.4 (lower part).

In our previous work [14], we have used the L-order statistics. In all phases of the applications, we have used various order statistics of the absolute values of the STFT with various window widths. Here, we use only one window function for the analysis. Then, after sorting the absolute STFT values and defining (by simply assuming, for example $Q = 50\%$, or calculating an adaptive threshold) the Q, we return back to perform all the calculations in the complex STFT domain. In this way, we obtain a very simple and efficient model for the calculation, while the results are improved with respect to those obtained by the procedure proposed in our previous work.

D. Algorithm for the Micro-Doppler Effects Removal

The simplest way to use the proposed method is in applying the L-statistics approach to all range bins, with a constant threshold, for example $Q = 50\%$. In this case the m-D will be separated, while the rigid body will not be degraded. In the case of impulse noise we will benefit from this procedure in each bin. Also, if there are close rigid body components, then this approach will help to resolve them, as it is described earlier. However, this way of calculation increases the calculation complexity.

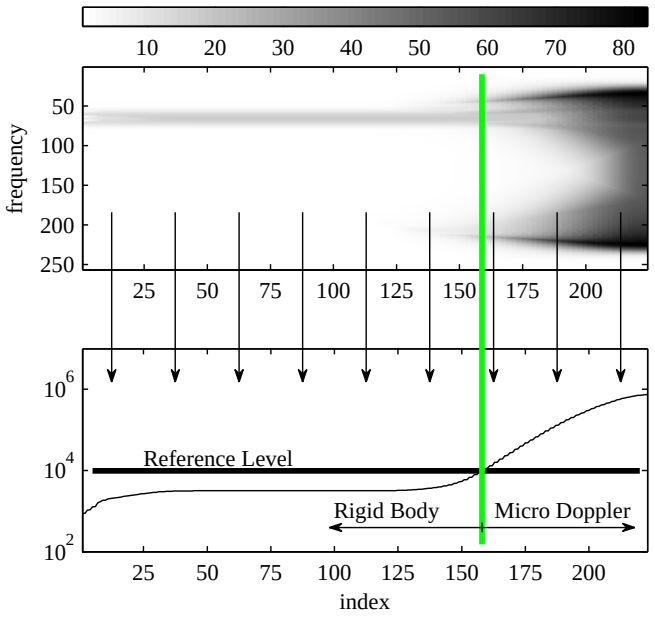

Fig. 4. Sorted STFT values, $|\Psi_k(m)|$, with a colorbar (upper). The values of $A(m)$, obtained by summing the squared values of the sorted STFT along the frequency, with the adaptive threshold R_L obtained based on the average value of 10% of its smallest values - thick horizontal line (lower).

In radar data analysis, only a part of the range bins may contain the m-D, while most of them will be m-D free. We can improve the calculation complexity by defining a procedure to avoid processing of the range bins where we can conclude that there is no target return or there is no m-D part of signal. If there is an m-D point, then a constant or adaptive threshold for the L-statistics application in the m-D removal could be used in order to separate the m-D, while most of the rigid body part of signal is preserved. If there is no m-D in the considered range bin, then processing for this range is not necessary. If the FT is already well focused, or if there is no returned target signal in the considered range bin, then the FT can be used as it is. Of course, this classification procedure is optional, and we will not lose anything in the radar image quality if we apply the presented method in some bins with already focussed image or where there is no target return. Thus, the thresholds in the next procedure may be chosen in quite a conservative way, to be sure not to miss any bin with m-D, allowing false m-D detections.

The range bins classification procedure will be presented as an algorithm.

The algorithm consists of the following steps:

Step 1: *Detect whether there is a returned target signal in the considered range bin, by using*

$$\max\{|S(k)|\} > \varepsilon, \tag{19}$$

where $\varepsilon = 0.02\max\{|S(k,l)|\}$ in the noiseless case or $\varepsilon = \max\{0.02\max\{|S(k,l)|\}, 2\sqrt{\sigma}/M\}$ in the presence of noise

(here $S(k,l)$ is the 2D FT of the received signal, i.e., full radar image matrix for all ranges and cross-ranges, while $S(k)$ is the radar image for a given range bin). The standard deviation σ of noise in the radar image, for a given range bin, can be estimated as [19]:

$$\hat{\sigma}_{re} = \frac{\text{median}\{|\text{Re}\{S(k)\} - \text{Re}\{S(k-1)\}|,\ k = 2,..,M\}}{0.6745\sqrt{2}}, \quad (20)$$

for the real part of $S(k)$. The same applies for the imaginary part. If there is no target in the returned signal, do not perform the following steps and take $S(k)$ as the radar image for the considered range bin. If there is a target signal, continue.

Step 2: *Detect whether there are any m-D effects in the considered range bin:*

$$R = \frac{\max\{|S(k)|\}}{\text{mean}\{|S(k)|\}} > 10.$$

The previous relation is the simplest concentration measure. In the case of a highly concentrated signal, R is close to M, while for a low concentrated signal, this value is close to 1. We say that the signal is well concentrated (rigid body only) if $R > 10$. This threshold was successfully tested for various scenarios and multi-component signals. If the signal is well concentrated take its FT $S(k)$ as the radar image for the considered range bin. If the signal is not well concentrated, continue.

Step 3: *Remove the m-D effects and reconstruct the FT of the reflectors that correspond to the rigid body in the considered range bin.* Remove the values of the STFT that are higher than the threshold and for each frequency sum the rest along the time. Take the obtained FT $S_L(k)$ (17) as the radar image for the considered range bin.

IV. Simulation Study

Example 1: The proposed method is tested on a signal with one rigid body point and four sinusoidally modulated components (used to model rotating reflectors),

$$s(m) = \sigma_B \sum_{i=1}^{K} \exp\{j y_{Bi} m\} + \sigma_R \sum_{i=1}^{P} \exp\{j[y_{R0i} m + A_{Ri} \sin(\omega_{Ri} m + \varphi_i)]\}, \quad (21)$$

with $K = 1$, $P = 4$, $\sigma_B = 1$, $\sigma_R = 3$, $y_{B1} = 0.4\pi$, $A_{Ri} = [96,\ 48,\ 64,\ 24]$, $\omega_{Ri} = \pi/128$, $y_{R0i} = \pi$ and $\varphi_i = 0$, for $i = 1,2,3,4$. The STFT of this signal is presented in Fig.5(a). The m-D, although moderate, significantly covers the rigid body, i.e., the part of the constant frequency component is almost invisible in the sinusoidal patterns. The sorted STFT is shown in Fig.5(b). Then, the highest STFT values are removed, for each frequency in the reconstruction phase. A constant threshold, with $Q = 60\%$ is used here. The FT reconstructed from the remaining STFT samples is shown in Fig.5(d). The rigid body is successfully reconstructed in the presence of the m-D. The original FT of the analyzed signal is given in Fig.5(c).

Example 2: Here, we analyze a signal with 10 components: $K = 5$ components with constant frequency (used to model rigid body reflectors) and $P = 5$ sinusoidally modulated components (used to model rotating reflectors), (21) with: $\sigma_B = 1$, $\sigma_R = 15$, $y_{Bi} = [1.9\pi,\ 1.95\pi,\ 2\pi,\ 2.05\pi,\ 2.1\pi]$, $A_{Ri} = [150,\ 300,\ 200,\ 440,\ 200]$, $\omega_{Ri} = [\pi/256,\ \pi/512,\ \pi/256,\ \pi/512,\ \pi/256]$, $y_{R0i} = 0$ and $\varphi_i = [0,\ -\pi/3,\ \pi/6,\ -2\pi/3,\ 0]$, for $i = 1,2,3,4,5$, $M = 1024$ and $M_w = 64$. The STFT of this signal is shown in Fig.6(a). The constant components, that correspond to the rigid body, are not well separated in the TF plane. Moreover, they are covered by the sinusoidally modulated patterns which represent the m-D effects of the rotating reflectors. If we sort the STFT values along time axis, then the representation of the rigid body parts does not change, since it is constant during the whole CIT, Fig.6(b). On the other hand, the fast rotating parts occupy only a small time intervals over a wide region of frequencies. They lie in high value regions of the sorted transform. Thus, they will be eliminated by removing the highest STFT values, for each frequency. An adaptive threshold, with $T_{hr} = 5$ is used here. The results are not sensitive to the value of T_{hr}. The reconstructed FT, obtained by summing the rest of the STFT (17) along the time is shown in Fig.6(d). We can clearly see five peaks that correspond to the five rigid body reflectors. The original FT is shown in Fig.6(c). It cannot be used even to determine the number of components in the analyzed signal.

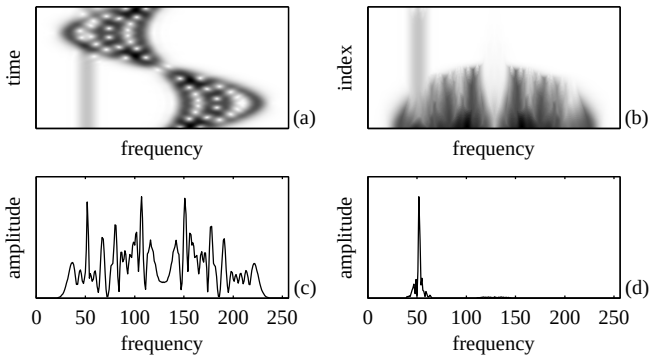

Fig. 5. (a) The STFT of a signal consisting of one rigid body component and four sinusoidally modulated components. (b) The sorted STFT of the same signal. (c) The original FT of the signal. (d) The FT of rigid body, reconstructed by summing the STFT values remaining after sorting and eliminating samples that correspond to the m-D effect.

Helicopter Data Analysis

Example 3: In this example, we first present a new simulation approach to the data of a German Air Force Bell UH-1D Helicopter known also as 'Iroquois' presented in [14]. Here, the simulation is performed according to the variable flashing reflection coefficients, rather than just by using a mathematical form that would produce the data as in [1]. Several effects are emphasized in the TFR Fig.7(a). The stationary patterns along the time-axis correspond to the rigid body reflection. The motion of two main blades is modeled by two rotating reflectors, producing sinusoidal FM signals with a large magnitude in the frequency direction, (23). The main rotor flashes are simulated by signals producing lines that connects extreme

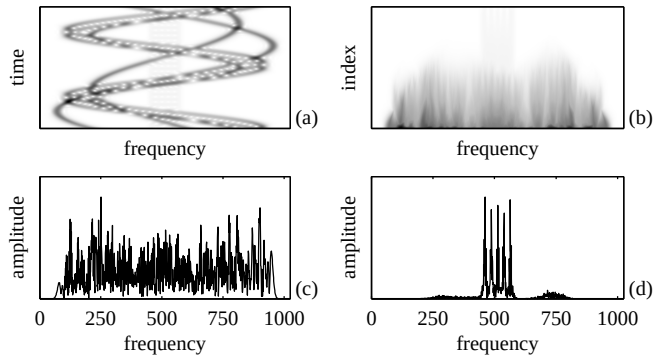

Fig. 6. (a) The STFT of a signal consisting of five rigid body components and five sinusoidally modulated m-D components (b) The sorted STFT of the same signal. (c) The original FT of the signal. (d) The FT of rigid body, reconstructed by summing the STFT values remaining after sorting and eliminating samples that correspond to the m-D effect.

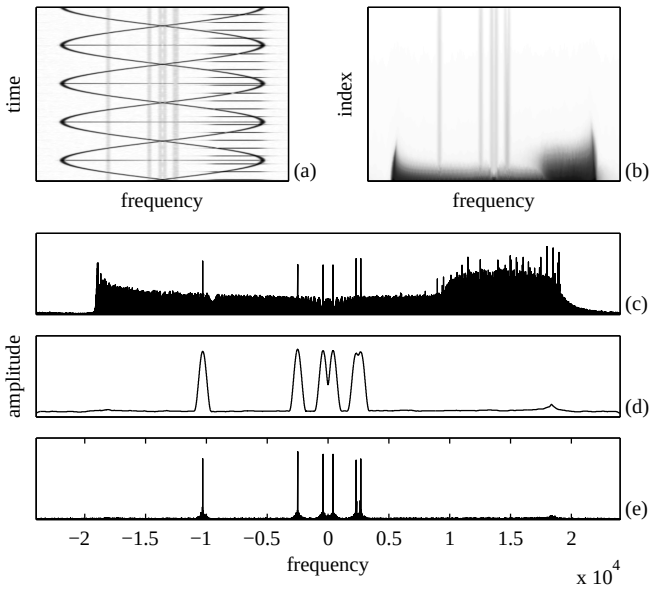

Fig. 7. (a) The STFT of a simulated signal of a German Air Force Bell UH-1D Helicopter. (b) The sorted STFT of this signal. (c) Original FT of the signal. (d) The FT of the rigid body, reconstructed by summing the lowest absolute STFT values. (e) The FT of the rigid body, reconstructed by the proposed method.

points of the sinusoidal FM signal, along the time axis. The smaller pulses that can be seen on the right-hand side of Fig.7(a) correspond to the tail rotor flashes, and they are simulated here by taking into account the physical meaning of its appearance. Namely, these flashes correspond to the periodic alignment of the main and tail rotors to maximally reflect the radar signal when they are normal to the line-of-sight. Therefore, we use here an angle dependent reflection coefficient

$$\sigma(t) = \exp(-30\,|\sin(2\pi t/T_{Rot})|), \tag{22}$$

where the reflection takes value 1 when $t = kT_{Rot}/2$ and $|\sin(2\pi t/T_{Rot})| = 0$, while for other t, $30|\sin(2\pi t/T_{Rot})|$ assumes high values and the reflection coefficient is small. Note that other effects that can be observed in a radar image, including multi-path, are not considered here.

The simplified model of the reflected UH-1D signal can now be written as

$$s(t) = x_{RIG}(t) + x_{ROT}(t) + x_{FL\_M}(t) + x_{FL\_T}(t),$$

where $x_{RIG}(t)$, $x_{ROT}(t)$, $x_{FL\_M}(t)$ and $x_{FL\_T}(t)$ represent signals caused by the rigid body, rotation of the main rotor, and the main and tail rotor flashes, respectively. The signal is considered within the interval of 400 ms, sampled with a rate of $\Delta t = 1/48$ ms. Four sinusoidal components, caused by the rigid body, are at the frequencies −10.3 kHz, −2.5 kHz, 2.3 kHz and 2.7 kHz. Two components at −0.4 kHz and 0.4 kHz correspond to the modulated time tones commonly added to the data tape [23]. The sinusoidal FM signals, corresponding to the rotation of the main rotor blades, are modeled as

$$x_{ROT}(t) = \sigma_{ROT}[e^{j2\pi A_{ROT}\sin(2\pi t/T_{ROT})} + e^{-j2\pi A_{ROT}\sin(2\pi t/T_{ROT})}], \tag{23}$$

where $\sigma_{ROT} = 10$, $T_{ROT} = 175$ ms and $A_{ROT} = 529.19$. The main and tail rotor flashes are modeled as

$$x_{FL\_M}(t) = 2.5\sum_{k=1}^{128}\frac{k+64}{128}e^{-30|\sin(2\pi t/175)|} \times \cos(25.98k\sin(\frac{2\pi t}{175})),$$

and

$$x_{FL\_T}(t) = 2.5\sum_{k=64}^{128} e^{-30|\sin(2\pi t/35.8)|}e^{(j(2.66k\sin(4\pi t/35.8)))}.$$

The signal is corrupted by a moderate Gaussian noise. To compare our simulation with the real one (for the m-D and rigid part values ratio) refer to [1], [23].

The proposed algorithm for the rigid body separation is applied to the simulated helicopter signal. The sorted STFT is shown in Fig.7(b). We can see that the STFT values corresponding to the rotating parts are in the high value region. The reconstructed FT is shown in Fig.7(e). All 5 reflectors that correspond to the rigid body are successfully recovered. The original FT is presented in Fig.7(c), while the reconstructed FT obtained by summing the absolute values of the remaining STFT samples is presented in Fig.7(d).

High-Resolution Analysis

Example 4: Two very close rigid body reflectors in the presence of m-D effects are simulated in this example

$$s(m) = e^{-j201\pi m/M} + e^{-j205\pi m/M} + 10e^{j58\cos(2\pi m/M)},$$

where $M = 256$ samples are used. The window with $M_w = 32$ zero-padded to M is used for the STFT calculation. The STFT of the analyzed signal is presented on Fig.8(a), while the sorted STFT is presented on Fig.8(b). It can be seen in Fig.8(a), that there are time instants when the STFTs of the close components are summed with opposite phase,

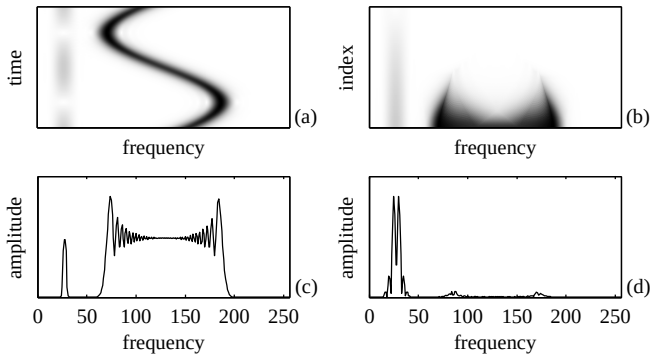

Fig. 8. (a) The STFT of a signal consisting of two very close components with constant frequency and one sinusoidally modulated component. (b) The sorted STFT of the same signal. (c) The original FT of the signal. (d) The FT of rigid body, reconstructed by summing the lowest STFT values.

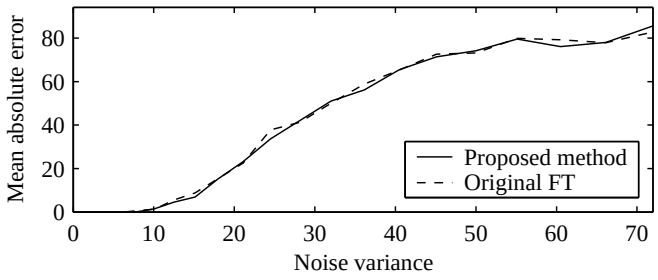

Fig. 9. Mean absolute error as a function of noise variance calculated for the case of one rigid body reflector without m-D. The solid line corresponds to the proposed method, while the dashed line corresponds to the full FT.

and they appear as separated. On the other hand, when the close components are summed in phase, they are not separated. Moreover, as it can be seen from the sorted STFT, presented in Fig.8(b), when the STFTs are summed in phase, the resulting STFT is higher. Consequently, by removing the highest values of the STFT, the remaining lower values are well separated; thus, the close components are separated. The FT reconstructed by summing over time 50% of lowest samples of the STFT, is shown in Fig.8(d), while the original FT is shown in Fig.8(c). We can see that the separation of the close components is achieved by the proposed method, although it is not possible in the original FT (the distance between two maxima positions is biased).

Noise Influence Analysis

Example 5: One stationary reflector and one m-D reflector are considered. Complex valued, white Gaussian noise $\varepsilon(t)$, with variance σ_ε^2, is added

$$s(m) = e^{-j0.75\pi m} + \sigma_R e^{j58\cos(2\pi m/256)} + \varepsilon(t),$$

where σ_R is the reflection coefficient of the m-D reflector. The noise variance is varied within a wide range $0 \le \sigma_\varepsilon^2 \le 72$ (from the case without noise up to the case when noise dominates), with step 1. For each variance value from this range, 1000 Monte Carlo simulations are performed. In each realization, we have found a position of the maximum in the L-statistics based estimate of the FT, $S_L(k)$. Then, the error is calculated as a difference of this position and the true signal frequency. The mean absolute error is calculated for each variance for 1000 realizations and the mean absolute error is plotted for various noise variance values. For the rigid body FT reconstruction we used, for each frequency, 50% of the smallest STFT values in the L-statistics summation.

We start with the case of pure stationary point $\sigma_R = 0$, to see how the L-statistics approach, with 50% of values, influences the results. It is well known that the FT transform is theoretically the best (ML) estimator for a pure sinusoid in Gaussian noise. The corresponding mean absolute error is depicted in Fig.9. The solid line corresponds to the proposed method, while the dashed line corresponds to the full FT. The FT is well reconstructed with the proposed L-statistics based method and the estimation results are not degraded with respect to the full FT, in this simple case, when the FT is the ML estimator.

We have analyzed noise influences in the case of $\sigma_R = 5$, as well. For the noiseless case, the STFT is shown in Fig.10(a), while the sorted STFT is shown in Fig.10(b). The original FT is presented in Fig.10(c). The FT reconstructed by summing, for each frequency, 50% of the lowest STFT samples is shown in Fig.10(d). The same plots for the case of $\sigma_\varepsilon^2 = 4.5$, $SNR = -6.53$ dB are shown in Fig.10(e–h). The signal to noise ratio (SNR) is calculated as the rigid body part of the signal to the noise ratio, in all cases. We can see that the proposed method successfully reconstructs the FT of the rigid body in the presence of m-D and noise.

The mean absolute error of the proposed method and the original FT is shown in Fig.10(i). The proposed method does not only reconstruct the FT successfully, but also eliminates the m-D effect and outperforms the original FT, whose estimation performance is degraded by the m-D effect.

Example 6: We analyzed one more case of one stationary reflector and one m-D reflector in the presence of noise. Here, the m-D reflector is stronger and closer to the stationary one. The corresponding signal is of the same form as in the previous example, but with $\sigma_R = 10$, while the rigid body reflector signal component is at the frequency $f_B = 0.125$ Hz. The same statistical analysis and reconstruction procedure as in the previous example are performed.

For the noiseless case, the STFT is shown in Fig.11(a), while the sorted STFT is shown in Fig.11(b). The original FT is presented in Fig.11(c). The FT reconstructed by summing, for each frequency, 50% of the lowest STFT samples is shown in Fig.11(d). The same plots for the case of $\sigma_\varepsilon^2 = 4.5$, $SNR = -6.53$ dB are shown in Fig.11(e–h). We can see from Fig.11(d) and Fig.11(h) that the performance of the proposed method does not degrade even in the case of strong m-D reflector positioned close to the rigid body reflector; in this case, the stationary and m-D components are crossing in the STFT, Fig.11(a) and Fig.11(e). The proposed method continues to successfully reconstruct the FT of the rigid body in the presence of noise, Fig.11(h), while the FT is not even able to indicate that there is a rigid body reflector, at all, Fig.11(g).

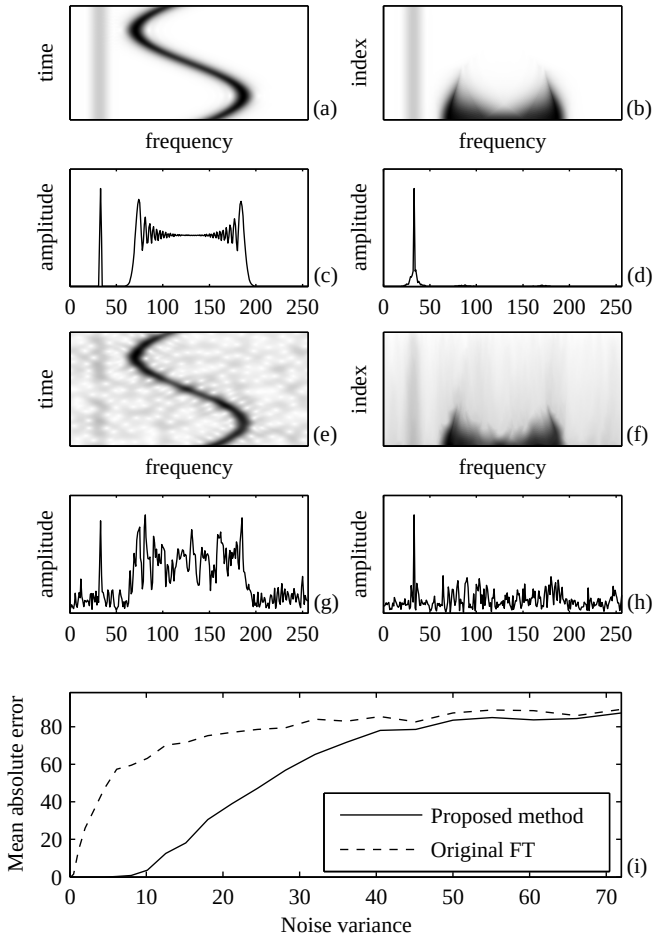

Fig. 10. One rigid body reflector and one m-D reflector. Noiseless case (a–d): (a) The STFT absolute value, (b) Sorted STFT, (c) The original FT, (d) Reconstructed FT. A realization of noisy case with $\sigma_\varepsilon^2 = 4.5$ (e–h): (e) The STFT absolute value, (f) Sorted STFT, (g) The original FT, (h) Reconstructed FT. (i) Mean absolute error as a function of noise variance in 1000 noisy realizations.

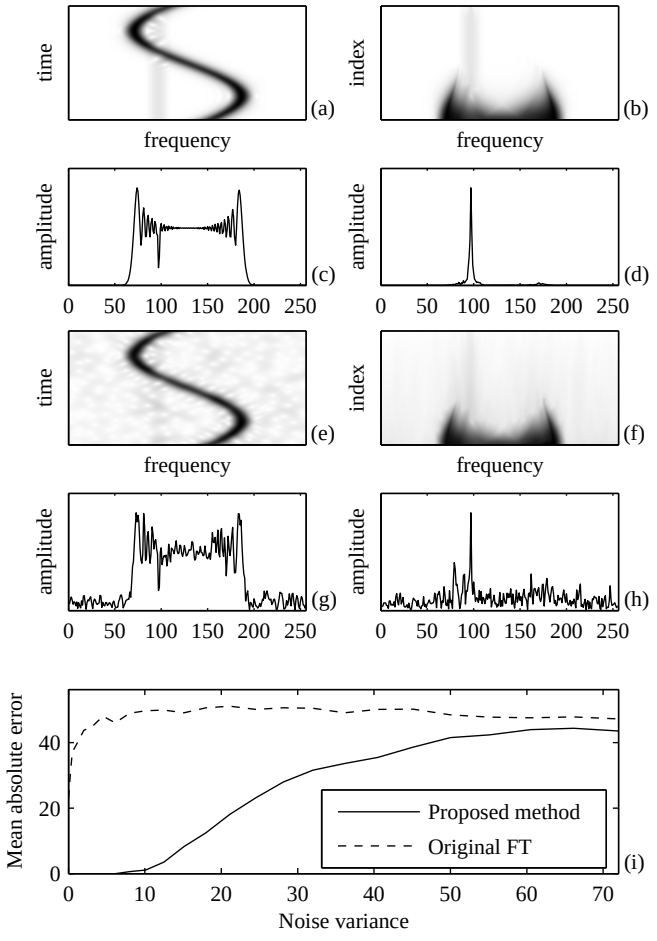

Fig. 11. One rigid body reflector and one close m-D reflector. Noiseless case (a–d): (a) The STFT absolute value, (b) Sorted STFT, (c) The original FT, (d) Reconstructed FT. A realization of noisy case with $\sigma_\varepsilon^2 = 4.5$ (e–h): (e) The STFT absolute value, (f) Sorted STFT, (g) The original FT, (h) Reconstructed FT. (i) Mean absolute error, in 1000 noisy realizations, as a function of noise variance.

The mean absolute error of the proposed method and the original FT are shown in Fig.11(i). From the presented statistics, we can confirm that, even in the presence of noise and close reflectors with strong m-D effects, the proposed method successfully reconstructs the FT of the rigid body, while the original FT completely fails to indicate the rigid body existence.

Non-Compensated Rigid Body Acceleration

Example 7: In this case an accelerating rigid body target is considered and examined. The received radar signal that corresponds to an accelerating target in the ISAR systems is a linear FM signal. Similarly, in SAR systems the target motion may induce linear frequency modulation in the received radar signal [17]. Therefore, we simulated three rigid body reflectors as three linear FM components with the chirp-rate a. In order to show that our algorithm will not remove only the m-D induced by vibrating and rotating targets, here we have also used a more complex form of the m-D. In this example, we will show that the algorithm is robust to the effects of acceleration.

The STFT of the analyzed signal is presented in Fig.12(a). We can clearly see that, as a result of the acceleration, the TFR of the rigid body part of the signal is not stationary during the time. Consequently, it is difficult to separate it from the m-D in the sorted STFT, Fig.12(b). Namely, if we perform the m-D separation by removing 50% of the highest STFT samples, as we did in the examples where there was no need for the motion compensation, we would reconstruct the FT of the rigid body as presented in Fig.12(d). Here, we have removed a significant part of the rigid body points, as well.

In the analysis of the rigid body with uncompensated acceleration, we should first compensate the remaining acceleration. This is not possible in the original signal, since the m-D signatures prevent us from properly compensating the remaining acceleration. However, the application of the proposed method for the m-D removal can solve this problem, as well. We will use the Local Polynomial Fourier Transform (LPFT)

$$LPFT(t,\Omega) = \int_{-\infty}^{\infty} s(\tau)\, w(\tau - t)\, e^{-j(\Omega\tau + \alpha\tau^2)}\, d\tau, \qquad (24)$$

instead of the STFT, where the term $exp(-j\alpha\tau^2)$ is used to compensate the linear frequency modulation of the rigid body part of the signal, $LPFT(t,\Omega) = FT\{s(\tau)e^{-j\alpha\tau^2}w(\tau-t)\}$. The parameter α is not known in advance, but we know that it can take values from a set $\Lambda = [-\alpha_{\max}, \alpha_{\max}]$, where $\alpha_{\max}$ is the chirp rate corresponding to the maximal expected acceleration (positive or negative), [24]. In this example we used $\Lambda = [-2 : 0.25 : 2]$. Now, $\hat{\alpha}$ can be estimated as the value from the set Λ for which we obtain the highest concentration of the reconstructed rigid body (compensated FT) based on the LPFT and the L-statistics, with, for example, $Q = 50\%$. The reconstructed FT, by using 50% of the lower LPFT values, will be denoted by $S_{L,\alpha}(k)$. Its concentration is calculated using the time-frequency concentration measure [25],

$$H(\alpha) = \left(\sum_{k=0}^{M-1} \left| S_{L,\alpha}(k) \right|^{1/p} \right)^{p}, \tag{25}$$

with $p = 1$. The LPFT, calculated with the estimated optimal value of $\hat{\alpha} = 1.25$, which results from $H(\alpha)$, is shown in Fig.12(e). The linear frequency modulation is compensated by $\hat{\alpha}$ in (24). Thus, with optimal $\hat{\alpha}$ we have components with almost constant frequency in the TFR representation of the rigid body reflectors. In this way, we have successfully reconstructed the rigid body and removed the m-D part, as it is presented in Fig.12(h). The procedure is not too sensitive to $\hat{\alpha}$. Very good results are obtained with neighboring values $\hat{\alpha} = 1.0$ and $\hat{\alpha} = 1.5$.

Note, that it would be impossible to estimate the chirp-rate $\hat{\alpha}$ from the original signal, without employing the proposed algorithm for the m-D removal.

Real Data Application

Example 8: The proposed algorithm is tested on real data in this example. The examined data were collected using an X-band radar operating at 9.2 GHz, [15]. The first real data represent three corner reflectors rotating at approximately 60 RPM (rotation per minute) and the rigid body observed by the radar with $T_r = 1$kHz. The STFT of the returned signal, for the given range bin, is shown in Fig.13(a). After sorting the STFT over time Fig.13(b), the constant frequency component corresponding to the rigid body becomes more visible, since the time varying frequency content is spread over many frequencies, for each frequency bin. The rigid body is separated from the m-D and its FT is successfully reconstructed by using 50% of the lowest STFT values, as shown in Fig.13(d). If we compare it to the FT of the original signal, Fig.13(c), we can see the improvement in the rigid body presentation.

In the second example, the real radar data corresponding to two outside corner reflectors, rotating at approximately 40 RPM (all facing radar) with rigid body, are analyzed. The same radar as in the previous example is used, while the reflectivity of rigid body is much higher than those of the rotating reflectors. The STFT representation of the observed signal is shown in Fig.13(e). The sorted STFT is shown in Fig.13(f). The original FT is shown in Fig.13(g). The reconstructed FT, obtained by summing 50% of the lowest STFT values is presented in Fig.13(h). We have successfully removed most of the m-D. Moreover, we may use the removed STFT samples in order to estimate features of rotating reflectors. Here, we have used a logarithmic scale to present the reconstructed values, since the m-D values were very low.

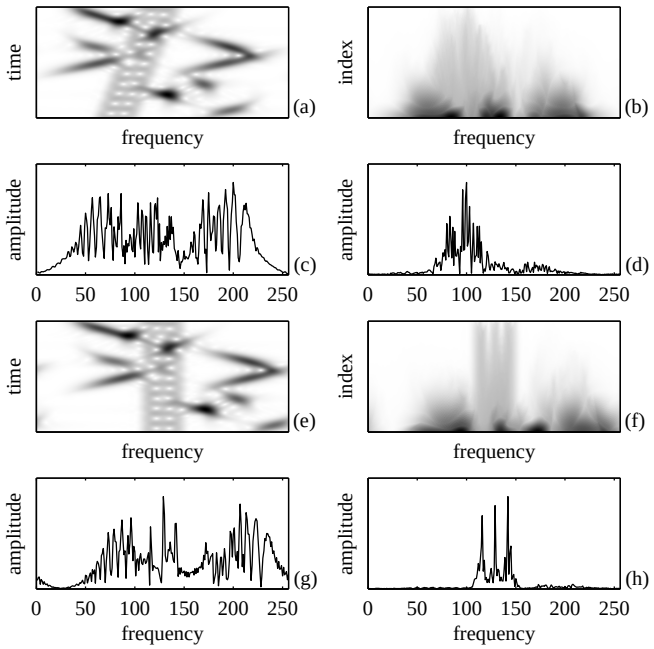

Fig. 12. Accelerating rigid body with a complex form of the mD. (a) TFR of the signal without motion compensation. (b) Sorted TFR of the original signal. (c) Original FT of the analysed signal. (d) Reconstructed FT of the accelerating rigid body without motion compensation. (e) TFR of the signal after motion compensation. (f) Sorted TFR of acceleration compensated signal. (g) The FT of the original signal with motion compensation. (h) Reconstructed FT of the accelerating rigid body with motion compensation.

V. CONCLUSION

The micro-Doppler effect appears in the ISAR/SAR images in the case when there are fast moving reflectors in the observed scene. The m-D can severely decrease the quality and readability of the obtained radar image. Its detection and removal is very important for obtaining focused image of the rigid body. In the paper, an algorithm for the m-D removal and reconstruction of the rigid body image is proposed. It is based on the L-statistics. Although the L-statistics are already applied by the authors for a similar purpose, the algorithm proposed here is simpler and produces better results. The reconstruction is performed by using only one complex STFT, rather than using several STFTs (with absolute values) and order statistics combination, as it was done in the previous work. Since the proposed algorithm is based on the L-statistics, being a tool for robust signal analysis, it is robust to the effects of noise. Also, it can behave as a high-resolution algorithm, since it can separate close rigid body points. In order to improve the computational efficiency, an adaptive threshold is used to distinguish among STFT samples that correspond to the rigid body and moving parts. Moreover, two additional

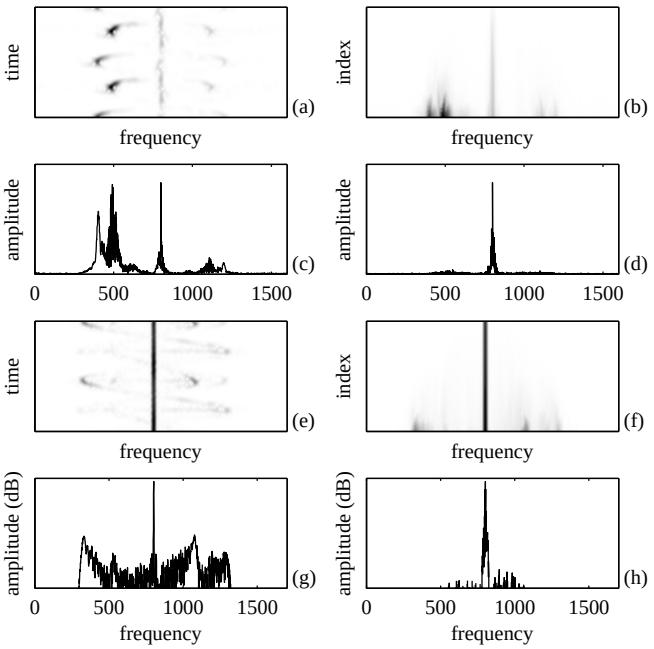

Fig. 13. Real radar data corresponding to a rigid body and three corner reflectors rotating at ~ 60 RPM (a–d). (a) the STFT. (b) Sorted STFT. (c) The original FT and (d) the FT reconstructed by summing over 50% of the lowest STFT samples. The same procedure is repeated for real radar data corresponding to a stronger rigid body and two corner reflectors rotating at ~ 40 RPM (e–h). A logarithmic amplitude scale is used in subplots (g) and (h).

thresholds are incorporated in the algorithm. The first threshold detects whether there is a returned radar signal in a range bin, while the second threshold detects whether there exist m-D effects in a range bin. Consequently, the procedure for the m-D extraction could be performed only for the range bins where the m-D effect is detected; that could lead to the overall computational savings. A procedure for the reconstruction of rotating points FT in the case of flashes is proposed. Through the examples, it is shown that the proposed algorithm successfully separates the rigid body and the m-D effects.

REFERENCES

[1] V. C. Chen, F. Li, S.-S. Ho, H. Wechsler: "Analysis of micro-Doppler signatures," *IEE Proc. Radar, Sonar, Navig.*, Vol. 150, No. 4, pp. 271-276, Aug. 2003.

[2] V. C. Chen: "Micro-Doppler effect in radar: Part I: Phenomenon, physics, mathematics, and simulation study," *IEEE Trans. on Aerosp. Electron. Syst*, Vol. 42, No. 1 Jan 2006.

[3] X. Bai, F. Zhou, M. Xing and Z. Bao: "High resolution ISAR imaging of targets with rotating parts," *IEEE Trans. on Aerosp. Electron. Syst*,Vol. 47, No. 4, pp. 2530 - 2543, Oct. 2011.

[4] F. Totir and E. Radoi: "Superresolution algorithms for spatial extended scattering centers," *Digital Signal Processing,* Vol. 19, No. 5, pp.780-792, Sept. 2009.

[5] M. Martorella: "Novel approach for ISAR image cross-range scaling," *IEEE Trans. Aerosp. Electron. Syst.*, Vol. 44, No. 1, pp. 281–294, 2008.

[6] M. Martorella and F. Berizzi: "Time windowing for highly focused ISAR image reconstruction," *IEEE Trans. Aerosp. Electron. Syst.*, Vol. 41, No. 3, pp. 992–1007, 2005.

[7] Y. Wang and Y.-C. Jiang: "ISAR imaging of ship target with complex motion based on new approach of parameters estimation for polynomial phase signal," *EURASIP Journal on Advances in Signal Processing,* Vol. 2011 (2011), Article ID 425203, 9 pages.

[8] T. Sparr, B. Krane: "Micro-Doppler analysis of vibrating targets in SAR," *IEE Proc. Radar Sonar Navig.*, vol 150, no. 4, pp. 277-283, Aug. 2003.

[9] B. Lyonnet, C. Ioana and M. G. Amin: "Human gait classification using microDoppler time-frequency signal representations," *Radar Conference, 2010 IEEE*, pp. 915 - 919, 10-14 May 2010.

[10] T. Thayaparan, S. Abrol, and E. Riseborough: "Micro-Doppler feature extraction of experimental helicopter data using wavelet and time-frequency analysis," *RADAR 2004, Proc. of the International Conference on Radar Systems*, 2004.

[11] T. Thayaparan, S. Abrol, E. Riseborough, L. Stanković, D. Lamothe and G. Duff: "Analysis of radar micro-Doppler signatures from experimental helicopter and human data,", *IET Proceedings Radar Sonar Navig.*, Vol. 1, no. 4, pp. 288-299, Aug. 2007.

[12] J. Li, and H. Ling: "Application of adaptive chirplet representation for ISAR feature extraction from targets with rotating parts," *IEE Proc. Radar, Sonar, Navig.*, Vol.150, No.4, pp.284-291, August 2003.

[13] T. Thayaparan, P. Suresh and S. Qian: "Micro-Doppler Analysis of Rotating Target in SAR, IET Signal Processing," *IET Signal Processing*, Vol. 4, No. 3, pp 245-255, 2010.

[14] L. Stanković, T. Thayaparan, and I. Djurović, "Separation of target rigid body and micro-Doppler effects in ISAR imaging", *IEEE Trans. Aerosp. Electron. Syst.*, Vol. 41, No. 4. pp. 1496-1506, Oct. 2006.

[15] T. Thayaparan, L. Stanković and I. Djurović: "Micro-Doppler Based Target Detection and Feature Extraction in Indoor and Outdoor Environments," *J. of the Franklin Institute*, Vol. 345, No. 6, pp 700-722, Sept. 2008.

[16] I. Djurović, L. Stanković, J. F. Bohme: "Robust L-estimation based forms of signal transforms and time-frequency representations," *IEEE Trans. Signal Processing*, Vol. 51, No. 7, pp. 1753 - 1761, July 2003.

[17] V. C. Chen, H. Ling: *Time-frequency transforms for radar imaging and signal analysis*, Artech House, Boston, USA, 2002.

[18] Y. Wang, H. Ling, and V. C. Chen, "ISAR motion compensation via adaptive joint time-frequency techniques," *IEEE Trans. Aerosp. Electron. Syst.*, Vol. 38, No. 2, pp. 670-677, 1998.

[19] V. Katkovnik, L. Stanković, "Instantaneous frequency estimation using the Wigner distribution with varying and data driven window length", *IEEE Trans. Signal Processing*, Vol. 46, No. 9, pp.2315-2325, Sept. 1998.

[20] Peng-Yeng Yin, "A new circle/ellipse detector using genetic algorithms," *Pattern Recognition Letters*, Vol. 20, No. 7, pp. 731-740, July 1999.

[21] T. Thayaparan, L. Stanković, M. Daković, V. Popović: "Micro-Doppler parameter estimation from a fraction of the period," *IET Signal Processing*, Vol. 4, No. 3, pp. 201 - 212, Jan. 2010.

[22] J. Misiurewicz, K. Kulpa, and Z. Czekala: "Analysis of recorded helicopter echo", *IEE Radar 98, Proceedings*, pp. 449-453.

[23] S. L. Marple: "Special time-frequency analysis of helicopter Doppler radar data", in *Time-Frequency Signal Analysis and Processing*, ed. B. Boashash, Elsevier 2004.

[24] I. Djurović, T. Thayaparan, LJ. Stanković: "Adaptive local polynomial Fourier transform in ISAR", Journal of Applied Signal Processing, Vol. 2006, Article ID 36093, 2006.

[25] L. Stanković: "A measure of some time–frequency distributions concentration", Signal Processing, Vol. 81, No. 3, pp. 621-631, March 2001.

Ljubiša Stanković (*M'91–SM'96–F'12*) was born in Montenegro in 1960. He received the B.S. degree in EE from the University of Montenegro (UoM), the M.S. degree in Communications from the University of Belgrade and the Ph.D. in Theory of Electromagnetic Waves from the UoM. As a Fulbright grantee, he spent 1984-1985 academic year at the Worcester Polytechnic Institute, USA. Since 1982, he has been on the faculty at the UoM, where he has been a full professor since 1995. In 1997-1999, he was on leave at the Ruhr University Bochum, Germany, supported by the AvH Foundation. At the beginning of 2001, he was at the Technische Universiteit Eindhoven, The Netherlands, as a visiting professor. He was vice-president of Montenegro 1989-90. During the period of 2003-2008, he was Rector of the UoM. He is Ambassador of Montenegro to the UK, Ireland and Iceland. His current interests are in Signal Processing. He published about 350 technical papers, more than 120 of them in the leading journals, mainly the IEEE editions. Prof. Stanković received the highest state award of Montenegro in 1997, for scientific achievements. He was a member the IEEE SPS Technical Committee on Theory and Methods, an Associate Editor of the *IEEE Transactions on Image Processing*, the *IEEE Signal Processing Letters* and numerous special issues of journals. Prof. Stanković is an Associate Editor of the *IEEE Transactions on Signal Processing*. He is a member of the National Academy of Science and Arts of Montenegro (CANU) since 1996 and a member of the European Academy of Sciences and Arts.

Thayananthan Thayaparan earned a B.Sc. (Hons.) in physics at the University of Jaffna, Srilanka, an M.Sc. in physics at the University of Oslo, Norway in 1991, and a Ph.D. in atmospheric physics at the University of Western Ontario, Canada in 1996. From 1996 to 1997, he was employed as a Postdoctoral Fellow at the University of Western Ontario. In 1997, he joined the Defence Research and Development Canada - Ottawa, Department of National Defence, Canada, as a Defence Scientist. His research interests include advanced radar signal and image processing methodologies and techniques against SAR/ISAR and HFSWR problems such as detection, classification, recognition, and identification. His current research includes synthetic aperture radar imaging algorithms, time-frequency analysis for radar imaging and signal analysis, radar micro-Doppler analysis, and noise radar technology. Dr. Thayaparan is a Fellow of the IET (Institute of Engineering & Technology). Currently, he is an Adjunct Professor at McMaster University. Dr. Thayaparan received IET Premium Award for Signal Processing for the best paper published in 2009-2010. Dr. Thayaparan is currently serving in the Editorial Board of *IET Signal Processing*. He has authored or coauthored over 174 publications in journals, proceedings, and internal distribution reports. As a principal writer, he wrote 3 editorials for the international journals *IET Signal Processing* (Institute of Engineering and Technology) and *IET Radar, Sonar & Navigation*.

Miloš Daković was born in 1970, Nikšić, Montenegro. He received the B.S. degree in 1996, the M.Sc. degree in 2001 and the Ph.D. degree 2005, all at the University of Montenegro in EE. He is an associate professor at the University of Montenegro. His research interests are signal processing, time-frequency signal analysis and radar signal processing. He is a member of the Time-Frequency Signal Analysis Group (www.tfsa.ac.me) at the University of Montenegro where he was involved in several research projects supported by Volkswagen foundation, Montenegrian Ministry of Science and Canadian Government (DRDC).

Vesna Popović-Bugarin was born in 1978, in Podgorica, Montenegro. She received the B.S. degree in 2001, the M.S. degree in 2005, and the Ph.D. degree in 2009, all at the University of Montenegro, in EE. She is currently assistant professor at the Faculty of Electrical Engineering, University of Montenegro. Her research interests include time-frequency signal analysis, SAR/ISAR imaging, micro-Doppler analysis and parameter estimation. She has published 17 scientific papers (6 in international journals, 10 in international conferences and 1 in domestic conference). More information about Vesna Popović-Bugarin can be found on http://www.tfsa.ac.me/vesna.html.